minerals

MDPI

Article

Effects of NaOH Content on the Reduction Kinetics of Hematite by Using Suspension Magnetization Roasting Technology

Shuai Yuan [1,2], Xinyu Li [1,2], Xun Wang [1,2,*], Hao Zhang [1,2] and Yanjun Li [1,2]

[1] School of Resources and Civil Engineering, Northeastern University, Shenyang 110819, China
[2] National-Local Joint Engineering Research Center of High-Efficient Exploitation Technology for Refractory Iron Ore Resources, Shenyang 110819, China
* Correspondence: xunwangcc@163.com

Abstract: Red mud is a potential iron resource that needs to be urgently exploited and utilized. However, due to the properties of high alkalinity, fine particle size and complex mineral composition, the utilization of red mud is difficult. Focusing on red mud's prominent feature of high alkalinity, this paper studies the influence of NaOH content on the reduction kinetics of hematite, which is the main component of red mud. The results show that the conversion degree of hematite was strongly inhibited by NaOH, and the magnetization and specific magnetic susceptibility of reduction products was significantly decreased with the increase in NaOH content. Meanwhile, the results of the calculation of kinetics parameters demonstrate that the addition of NaOH did not affect the control step of the reduction of hematite, while it dramatically decreased the reduction rate of hematite. Moreover, thermodynamic analysis and SEM-EDS detection were conducted to uncover the inhibited mechanism of NaOH on the reduction of hematite, which indicated that sodium ferrite could be produced spontaneously under the experimental conditions and that it is hard for it to be further reduced by CO. Furthermore, the produced sodium ferrite formed a dense film, which covered the surface of the hematite particles, inhibiting the diffusion of CO and thereby hindering the reduction of the interior hematite.

Keywords: reduction kinetics; inhibited mechanism; sodium hydroxide; hematite; SMR technology

Citation: Yuan, S.; Li, X.; Wang, X.; Zhang, H.; Li, Y. Effects of NaOH Content on the Reduction Kinetics of Hematite by Using Suspension Magnetization Roasting Technology. *Minerals* **2022**, *12*, 1107. https://doi.org/10.3390/min12091107

Academic Editor: Mark I. Pownceby

Received: 30 June 2022
Accepted: 30 August 2022
Published: 30 August 2022

1. Introduction

Red mud, one of the major waste materials, is produced in the alumina extraction process. Due to its fine particle size, strong corrosivity and complex mineral composition, the efficient utilization of untreated red mud is hard to realize [1–3]. According to statistics, the global reserves of red mud have more than 4 billion tons, and it continues to grow by about 175.5 million tons per year [4,5]. As the largest producer of alumina, China possesses large quantities of red mud and the storage has exceeded 600 million tons. Furthermore, there are also over 100 million tons of red mud per year produced in China [5,6]. At present, land stockpiling is the main method to treat red mud. However, it results in a series of environmental–hydrogeological problems and destroys the balance of the ecological environment [7,8].

Red mud has a remarkable economic worth, since it contains abundant valuable metal elements such as iron, aluminum, vanadium and titanium [9–11]. Among these elements, the iron in high-iron red mud is usually more than 30%, which is higher than that of raw iron ore in the most Chinese mines. Therefore, the efficient recycling and utilization of iron from high-iron red mud has significant influence on the development of the national economy and the comprehensive improvement of the ecosystem environment.

In the last few decades, plenty of studies have been conducted to investigate the most efficient method of extracting iron from red mud. Among them, suspension magnetization roasting (SMR) developed by the Han research tem (Northeastern University) is regarded

as a potentially efficient method to treat refractory iron ore due to its low roasting temperatures, high quality, high energy utilization and lower pollution [12–16]. Liu et al. [17] studied the effect of SMR operation parameters on the recovery of iron from red mud in a laboratory, and it was found that a good indicator with iron recovery of 88.45% and iron grade of 56.41% was acquired under the optimized conditions of 540 °C roasting temperature, 15 min reduction time, 500 mL/min gas flow rate and 30% CO concentration. Moreover, the feasibility of the SMR technique for the extraction of iron from red mud was further verified by the semi-industrial scale test [18]. Even though these investigations have proposed and proved the advantages of the SMR technique for the recycling of red mud, the reduction mechanism, including kinetics, phase transformation and structure evolution, is still unclear. Particularly, the influence of alkali content on the reduction of red mud is not reported, which is a key factor to limit the recycling of the resource. The compositions of red mud are very complex, containing a variety of minerals [19]. According to the different compositions, red mud can be divided into different types. Regardless of types, however, the major mineral of red mud is hematite, and it is also the most useful mineral that is worth being recycled from the red mud. Therefore, the investigation of the influence of alkali content on the hematite can reflect the common problems within red mud reduction. In order to make the study more universal for all of the red mud resources, it is very meaningful to investigate the effects of NaOH content on the reduction of hematite.

In this paper, the effects of alkali content on the reduction kinetics of hematite were studied systematically by using SMR technology. In addition, the influence mechanism of alkali content on the reduction of hematite were uncovered by vibrating sample magnetometer (VSM), X-ray diffraction (XRD) and scanning electron microscopy (SEM).

2. Materials and Methods

2.1. Materials

The sample of pure hematite was obtained from Liaoning Province, China. The obtained sample was first picked by hand to remove a small amount of gangue minerals associated with hematite, and then the sample was crushed and ground to −0.5 mm. After that, the sample particles with different size fractions of −0.5 + 0.15 mm, −0.15 + 0.074 mm, −0.074 + 0.045 mm and −0.045 mm were acquired through wet-sieving. In order to simulate the reduction process of red mud ore, the size composition of the sample used in the reduction experiments consisted of −0.5 + 0.15 mm (13.68%), −0.15 + 0.074 mm (16.87%), −0.074 + 0.045 mm (22.69%) and −0.045 mm (46.76%). The chemical composition analyses and X-ray diffraction (XRD) detection were conducted to determine the purity of the sample [20–22], and the results are presented in Figure 1 and Table 1, respectively. From the results, it can easily be found that the purity of the hematite sample was 98.21%, which can meet the test requirements very well.

2.2. Methods

2.2.1. Experimental Apparatus and Procedure

The reduction experiments were performed in a vertical suspension furnace (OFT-1200X-S-VT, HFKJ, Hefei, China), and the schematic diagram of the experimental equipment is presented in Figure 2. For each experiment, 5 g hematite sample was first heated in the reaction tube to a desired temperature under a nitrogen flow of 100 mL/min. The heating speed was set as 15 °C/min. Once it reached the required temperature, the reducing gas mixture of 20 mL/min CO and 80 mL/min N_2 was introduced into the reaction tube, and the reduction process began. After reducing for a period of time, the pure nitrogen flow of 100 mL/min was introduced again to remove the remaining reducing gas in the reaction tube, and the reduction products were then cooled down to room temperature under the nitrogen conditions. Each set of tests was conducted three times, and the average was adopted as the reported result.

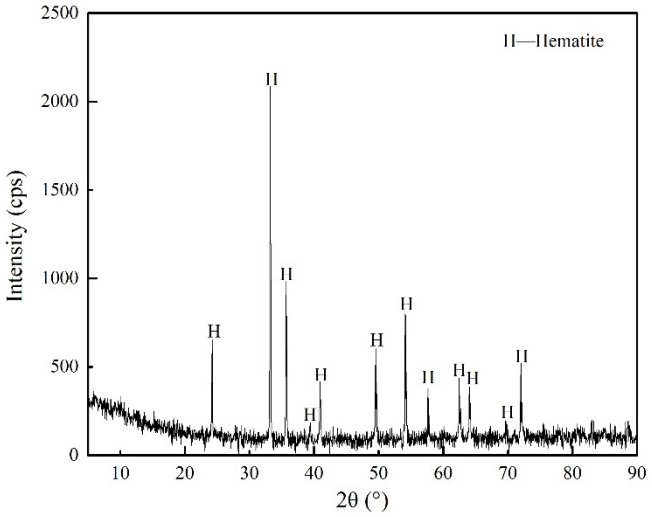

Figure 1. X-ray diffraction pattern of hematite.

Table 1. Chemical composition of hematite sample (mass, %).

Composition	TFe	FeO	SiO_2	Al_2O_3	CaO	MgO	P	S
Content	68.75	0.45	0.48	0.081	0.28	0.22	0.025	0.004

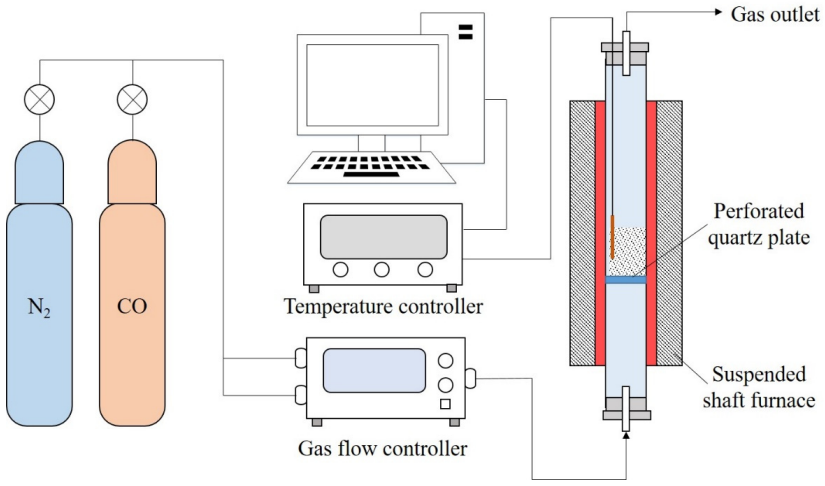

Figure 2. The schematic diagram of the experiment equipment.

2.2.2. Sample Characterization

In order to calculate the conversion of the reduction reaction, chemical analysis was adopted to determine the FeO content of reduction products. The detailed detection process was in accordance with our previous study [23]. X-ray diffraction detection (PW3040, Philips Co., The Netherlands) was used to characterize the phase transformation of the reduction products. VSM (JDAW-2000D) and SEM-EDS (JEM-3200FS) were adopted to analyze the changes in the mineral magnetism and microstructure of reduction products during the reduction process, respectively.

2.2.3. Dynamic Analysis Method

For hematite sample, the major reaction in the suspended reduction processing is the transformation of hematite to magnetite [24] (Equation (1)). The results from the chemical analysis indicate that the purity of the hematite sample is 98.21%; thus, 5 g experiment

sample contains 4.91 g hematite. According to the law of conservation of mass, the iron metal equilibrium is listed as Equation (2) to (4).

$$3Fe_2O_3(s) + CO(g) = 2Fe_3O_4(s) + CO_2(g) \quad (1)$$

$$m_{Fe_3O_4} = 4.75\alpha \quad (2)$$

$$m_{FeO} = \frac{72}{232} m_{Fe_3O_4} = 1.47\alpha \quad (3)$$

$$\omega_{FeO} = \frac{m_{FeO}}{m_{Fe_3O_4} + m_{Fe_2O_3} + 0.09} = \frac{1.47\alpha}{5 - 0.16\alpha} \quad (4)$$

where α refers the conversion of the reduction reaction, $m_{Fe_3O_4}$ presents the weight of the new producing of Fe_3O_4 in the sample (g), ω_{FeO} is the mass fraction of FeO in the sample (%), m_{FeO} is the weight of FeO in the sample (g), and $m_{Fe_2O_3}$ is the weight of Fe_2O_3 in the sample (g).

Based on Equation (4), the relation between α and ω_{FeO} can also be described as Equation (5). Therefore, α can be calculated based on the FeO analysis results.

$$\alpha = \frac{5\omega_{FeO}}{1.47 + 0.16\omega_{FeO}} \quad (5)$$

The reaction rate is measured by the change in conversion of the reduction reaction per unit time; thus, the reaction rate of the suspension reduction can be obtained through the conversion of the reduction reaction (α) and reaction time, and the kinetics equation of the isothermal dynamics also can be determined (Equation (6)) [25,26]. Moreover, the most probable mechanism function can be determined by the analysis of the linear correlation between the fitting line and the experimental data.

$$v = \frac{d\alpha}{dt} = k(T)f(\alpha) \quad (6)$$

where v is the reaction rate (s^{-1}), t is the reaction time (s), T is the temperature of the reaction (K) and k is the reaction rate constant, and it can be characterized by Arrhenius equation as [27,28]:

$$k(T) = A\exp(\frac{-E_\alpha}{RT}) \quad (7)$$

Herein, A is the pre-exponential factor (s^{-1}), E_α is the apparent activation energy (J/mol) and R is the gas constant (8.314 J/(mol·K)).

$$\ln k = \ln A - \frac{E_\alpha}{RT} \quad (8)$$

By taking the log of Equation (7), the formula transforms to Equation (8). From Equation (8), it can be seen that $\ln k$ is linearly related to $\frac{1}{T}$. Therefore, after carrying on the linear data fitting to the experimental findings, E_α and A can be obtained from the slope and intercept, respectively [27,28].

3. Results and Discussion

3.1. Influence of the NaOH Content on the Conversion Fractions of Hematite

Figure 3 shows the conversion degree of hematite versus reaction time under different reaction conditions. As shown in Figure 3, for a same amount of NaOH, the conversion degree and reduction rate of hematite increased with the increase in reduction temperature, which indicates that the increase in reduction temperature improved the activity of the reactants and promoted the reaction. On the other hand, the conversion degree of hematite decreased with the increasing amount of NaOH, and the reduction process of hematite was significantly prolonged with the increasing addition of NaOH at a constant reduction

temperature. These results indicate that the addition of NaOH could strongly hinder the conversion of hematite and thereby reduce its reduction. Moreover, it also could be found that the inhibition effects of NaOH on the reduction of hematite were more distinct in low-temperature conditions. For a deeper understanding of the effect of NaOH on the conversion of hematite during the suspension reduction process, the reduction products treated with different NaOH content were analyzed by XRD and VSM; the results are shown in Figures 4 and 5, respectively. As shown in Figure 4, the intensity of the magnetite diffraction peaks gradually decreased with the increase in NaOH content, while those of hematite continuously increased in intensity. These results confirmed that the conversion of hematite to magnetite was strongly inhibited by NaOH. A similar conclusion also could be drawn from Figure 5: with the increase in NaOH content, the magnetization and specific magnetic susceptibility of reduction products decreased, which would cause more hematite loss in the magnetic separation tailings.

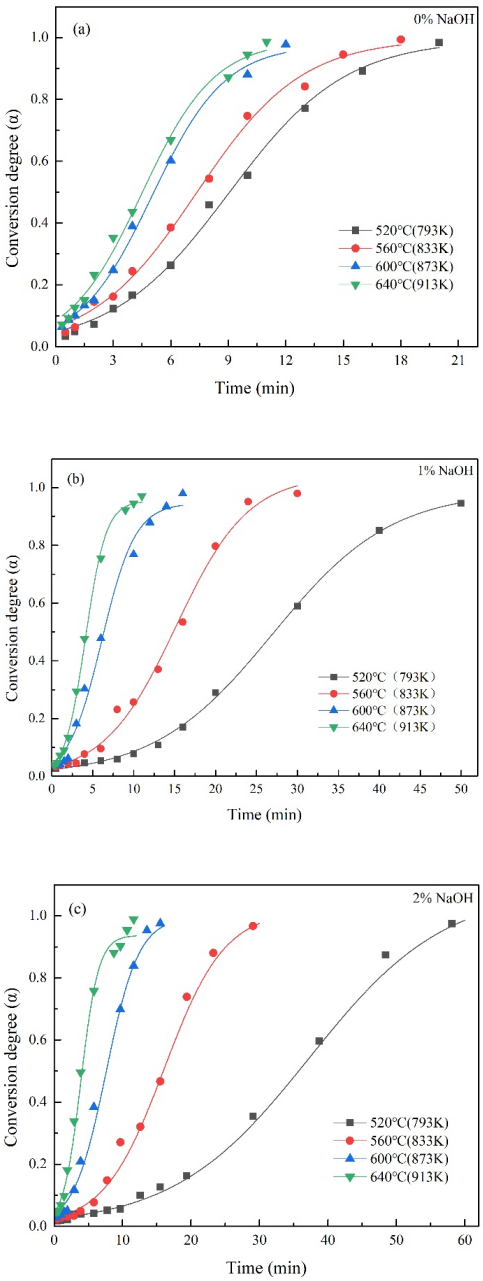

Figure 3. Conversion degrees of hematite under different conditions ((**a**) 0% NaOH, (**b**) 1% NaOH, (**c**) 2% NaOH).

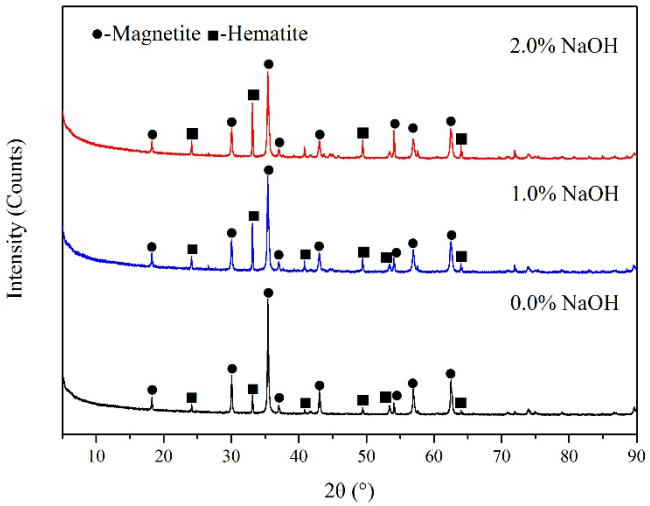

Figure 4. XRD patterns of reduction products with different NaOH content at 560 °C.

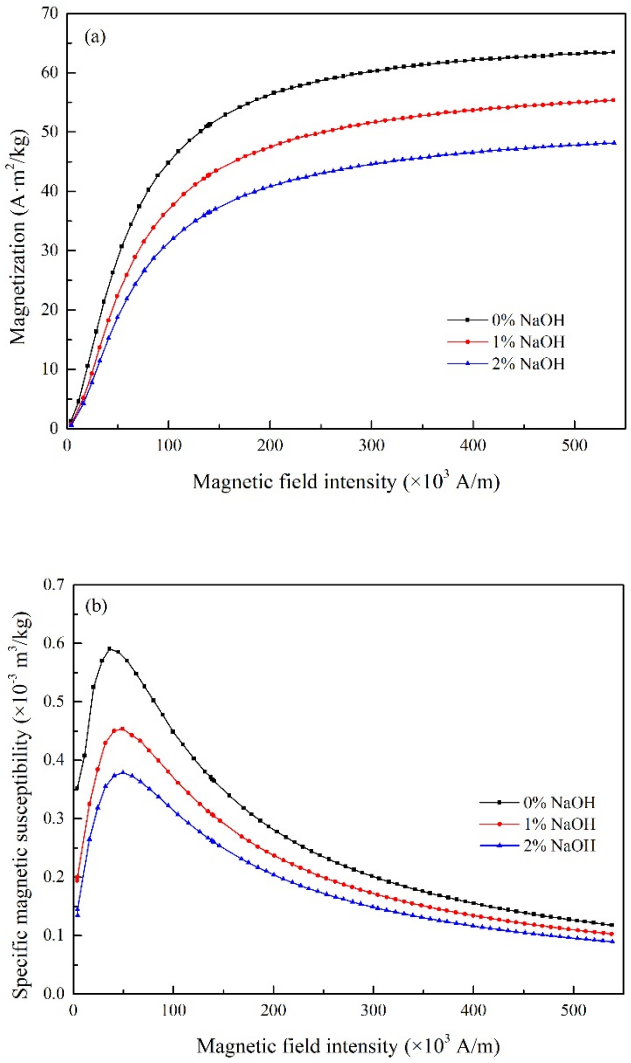

Figure 5. Magnetic intensity (**a**) and magnetic susceptibility (**b**) of reduction products with different NaOH contents at 560 °C.

3.2. Influence of NaOH Content on the Reduction Kinetics of Hematite

The results show in Section 3.1 illustrated that the addition of NaOH not only affected the conversion degree of hematite, but also influenced the reduction process of it. Reduction kinetics have been considered one of the most efficient ways to evaluate the reduction process, and it is very meaningful for the application of reduction kinetics to analyze the reduction behavior of the mineral and thereby to understand and optimize the reduction process. In this study, thirty common reduction kinetic models (Table 2) were used to fit and determine the most probable reduction mechanism model of hematite under different conditions [23].

Table 2. Description of the thirty kinetic models used in this study.

Mechanism Functions		$f(\alpha)$	$G(\alpha)$
Nucleation model	A1	$1-\alpha$	$-\ln(1-\alpha)$
	A2	$2(1-\alpha)[-\ln(1-\alpha)]^{1/2}$	$[-\ln(1-\alpha)]^{1/2}$
	A3	$3(1-\alpha)[-\ln(1-\alpha)]^{2/3}$	$[-\ln(1-\alpha)]^{1/3}$
	A4	$4(1-\alpha)[-\ln(1-\alpha)]^{3/4}$	$[-\ln(1-\alpha)]^{1/4}$
	A3/2	$3/2(1-\alpha)[-\ln(1-\alpha)]^{1/3}$	$[-\ln(1-\alpha)]^{2/3}$
	A1/4	$1/4(1-\alpha)[-\ln(1-\alpha)]^{-3}$	$[-\ln(1-\alpha)]^{4}$
	A1/3	$1/3(1-\alpha)[-\ln(1-\alpha)]^{-2}$	$[-\ln(1-\alpha)]^{3}$
	A1/2	$1/2(1-\alpha)[-\ln(1-\alpha)]^{-1}$	$[-\ln(1-\alpha)]^{2}$
Geometrical contraction models	R1/2	$1/2(1-\alpha)^{-1}$	$1-(1-\alpha)^{2}$
	R1/3	$1/3(1-\alpha)^{-2}$	$1-(1-\alpha)^{3}$
	R1/4	$1/4(1-\alpha)^{-3}$	$1-(1-\alpha)^{4}$
	R2	$2(1-\alpha)^{1/2}$	$1-(1-\alpha)^{1/2}$
	R3	$3(1-\alpha)^{2/3}$	$1-(1-\alpha)^{1/3}$
	R4	$4(1-\alpha)^{3/4}$	$1-(1-\alpha)^{1/4}$
Diffusion models	D1	$1/2\alpha^{-1}$	α^{2}
	D2	$[-\ln(1-\alpha)]^{-1}$	$A+(1-\alpha)\ln(1-\alpha)$
	D3	$(1-\alpha)^{1/2}[1-(1-\alpha)^{1/2}]^{-1}$	$[1-(1-\alpha)]^{1/2}]^{2}$
	D4	$3/2(1+\alpha)^{2/3}[(1+\alpha)^{1/3}-1]^{-1}$	$[(1+\alpha)]^{1/3}-1]^{2}$
	D5	$3/2(1-\alpha)^{4/3}[(1-\alpha)^{-1/3}-1]^{-1}$	$[(1-\alpha)]^{-1/3}-1]^{2}$
	D6	$3/2(1-\alpha)^{2/3}[1-(1-\alpha)^{-1/3}]^{-1}$	$[1-(1-\alpha)]^{1/3}]^{2}$
	D7	$6(1-\alpha)^{2/3}[1-(1-\alpha)^{-1/3}]^{1/2}$	$[1-(1-\alpha)]^{1/3}]^{1/2}$
	D8	$3/2[(1-\alpha)^{-1/3}-1]-1$	$1-2/3\alpha-(1-\alpha)^{2/3}$
Power laws	P4	$4\alpha^{3/4}$	$\alpha^{1/4}$
	P3	$3\alpha^{2/3}$	$\alpha^{1/3}$
	P2	$2\alpha^{1/2}$	$\alpha^{1/2}$
	P1	1	α
	P3/2	$2/3\alpha^{-1/2}$	$\alpha^{3/2}$
Reaction-order models	F1	$1-\alpha$	$-\ln(1-\alpha)$
	F2	$(1-\alpha)^{2}$	$(1-\alpha)^{-1}-1$
	F3	$1/2(1-\alpha)^{3}$	$(1-\alpha)^{-2}$

By comparing the linear coefficient between the experimental data and the fitting line, the most probable reaction model for the reduction of hematite at different additions of NaOH has been determined and the results are depicted in Figure 6 and Table 3. As shown in Table 3, the reduction processes of hematite with and without addition of NaOH were met well with the A3 reaction models of the nucleation model, and the control step of hematite reduction was not affected by the addition of NaOH. Meanwhile, it could also be seen that the reaction rate increased with the increase in temperature at a constant of NaOH content, which further confirmed that the increase in temperature facilitated and accelerated the reduction of hematite. However, for a similar temperature, the increasing addition of NaOH content would obviously inhibit the reduction of hematite, and the reaction rate of hematite significantly decreased, especially in low-temperature conditions.

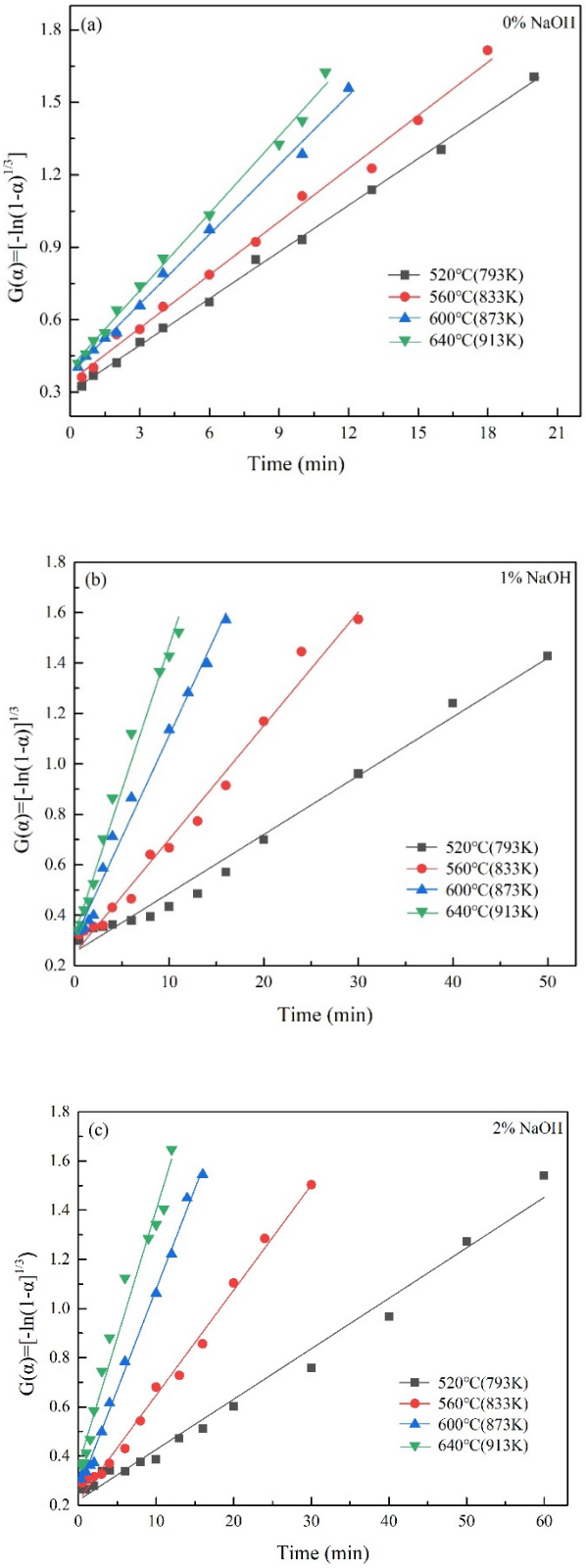

Figure 6. Linear regression analysis curves between mechanism function G(α) of A3 model and experimental data ((**a**) 0% NaOH, (**b**) 1% NaOH, (**c**) 2% NaOH).

Table 3. Reaction rate constant and linear correlation coefficient of reduction at different temperatures.

NaOH Additive	$G(\alpha)$	Temperature (k)	$1/T$	Reaction Rate (k/min^{-1})	ln$k$	R^2
0%	$G(\alpha) = [-\ln(1-\alpha)]^{1/3}$	793	0.000938	0.06435	−2.74342	0.99834
		833	0.000904	0.07337	−2.61224	0.99359
		873	0.000873	0.09599	−2.34351	0.99597
		913	0.000843	0.10640	−2.24055	0.99541
1%	$G(\alpha) = [-\ln(1-\alpha)]^{1/3}$	793	0.000938	0.02330	−3.7593	0.98532
		833	0.000904	0.04508	−3.09932	0.98583
		873	0.000873	0.08082	−2.51553	0.98907
		913	0.000843	0.10429	−2.16902	0.98568
2%	$G(\alpha) = [-\ln(1-\alpha)]^{1/3}$	793	0.000938	0.02052	−3.88636	0.98552
		833	0.000904	0.04275	−3.15239	0.99224
		873	0.000873	0.08178	−2.50372	0.99611
		913	0.000843	0.10369	−2.26635	0.97408

In order to better understand the influence of NaOH on the reduction of hematite, the apparent activation energy (E_α) and the pre-exponential factor (A) were also calculated by Equations (7) and (8), and the results are summarized as Figure 7. As shown in Figure 7, the apparent activation energy of the hematite reduction increased significantly after the addition of NaOH, which indicated that the reaction energy barrier for the reduction of hematite was improved by the addition of NaOH, and thus made it more difficult. Furthermore, the increase in the pre-exponential factor also demonstrated that the collision efficiency of the reactants was reduced and the reduction rate was decreased after the addition of NaOH.

3.3. Inhibited Reduction Mechanism Analysis

The above experiments and analyses demonstrated that the conversion of hematite to magnetite could be significantly inhibited by the addition of NaOH during the suspension reduction process, while the essential inhibition mechanism of NaOH on the reduction of hematite was still unclear. Herein, thermodynamic analysis and SEM-EDS detections were conducted to reveal this essential mechanism, the results are shown in Table 4, Figures 8 and 9. The thermodynamic date was calculated via the FactSage software. Figure 8 shows the relationship between the Gibbs free energy and temperature of the possible reaction equations in the process of suspension reduction. As shown in Figure 8, the ΔG of Equation (13) was less than zero, which indicates that sodium ferrite could be produced spontaneously in the experimental conditions. However, it was hard for the produced sodium ferrite to be reduced by CO because the ΔG of Equation (14) was much more than zero. Meanwhile, from Figure 9, it could be seen that the element of Na was evenly distributed in the hematite surface and it also coexisted with Fe closely, which further proved that sodium ferrite occurred during the suspension reduction process after the addition of NaOH. Moreover, Figure 9 also shows that the dense film of sodium ferrite was presented in the surface of hematite, which would inhibit the diffusion of CO and further hinder the reduction of hematite in the interior.

Table 4. Thermodynamic equations of suspension reduction of hematite after addition of NaOH.

Number	Equation
(9)	$3Fe_2O_3(s) + CO(g) = 2Fe_3O_4(s) + CO_2(g)$
(10)	$Fe_3O_4(s) + CO(g) = 3FeO(s) + CO_2(g)$
(11)	$Fe_3O_4(s) + 4CO(g) = 3Fe(s) + 4CO_2(g)$
(12)	$FeO(s) + CO(g) = Fe(s) + CO_2(g)$
(13)	$2NaOH(s) + Fe_2O_3(s) = Na_2O{\cdot}Fe_2O_3(s) + H_2O(g)$
(14)	$3Na_2O{\cdot}Fe_2O_3(s) + CO(g) = 2Fe_3O_4(s) + 3Na_2O(s) + CO_2(g)$

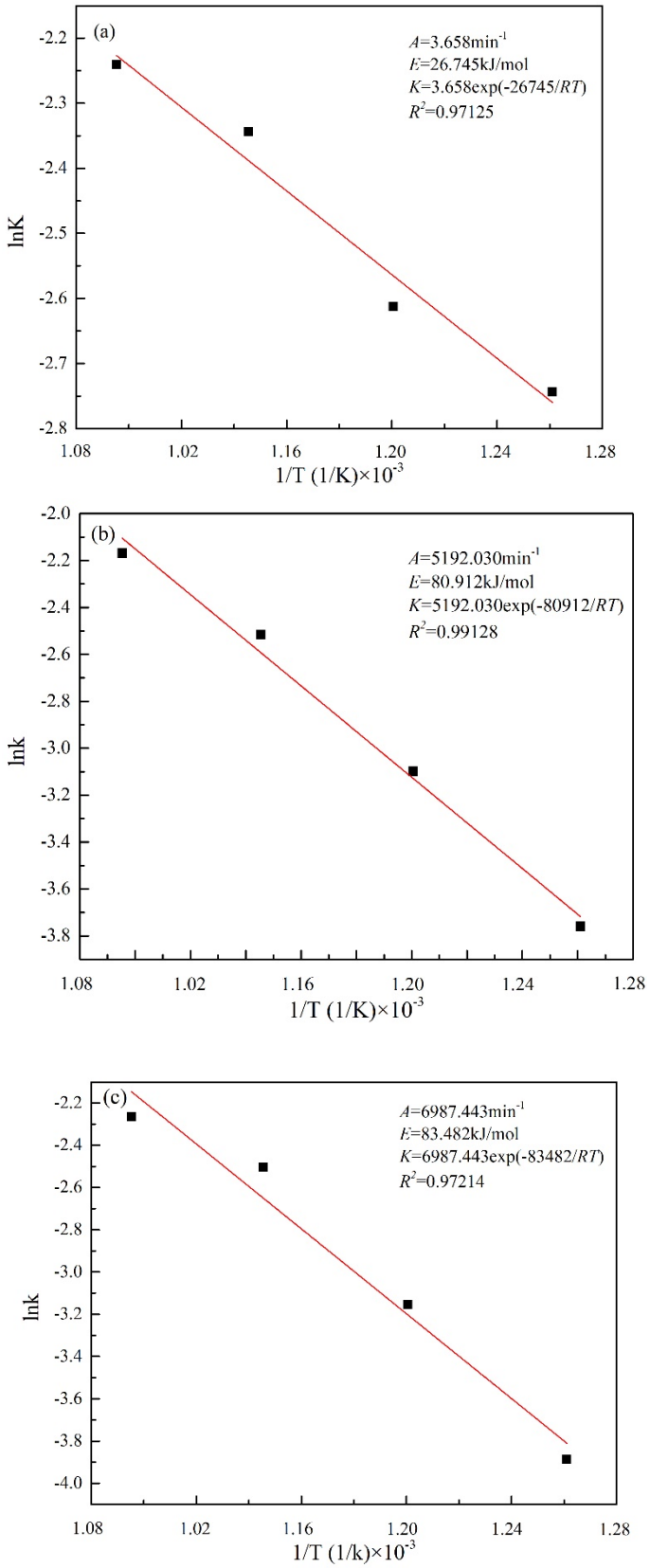

Figure 7. Arrhenius plot for the evaluation of the activation energy of the process (**a**) 0% NaOH, (**b**) 1% NaOH, (**c**) 2% NaOH.

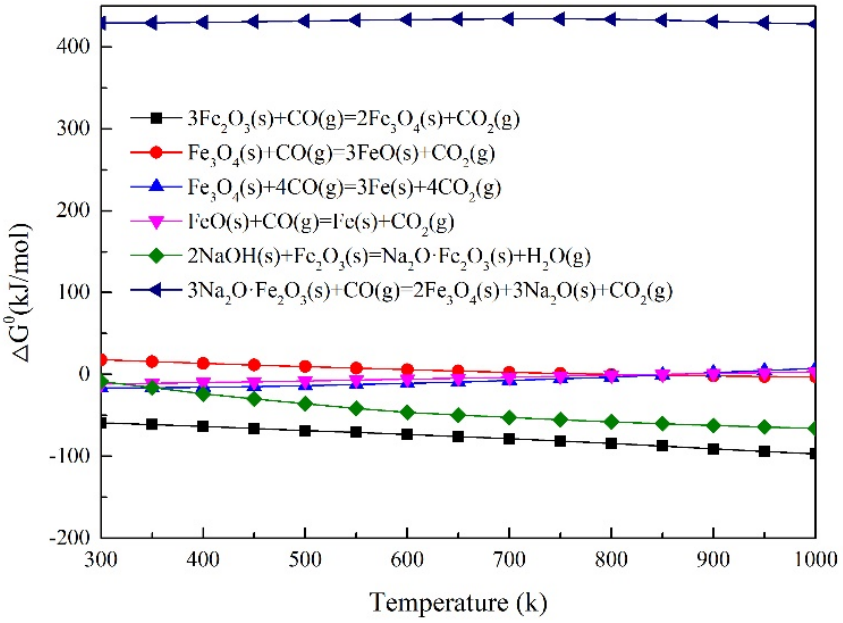

Figure 8. Thermodynamic analysis of suspension reduction of hematite after addition of NaOH.

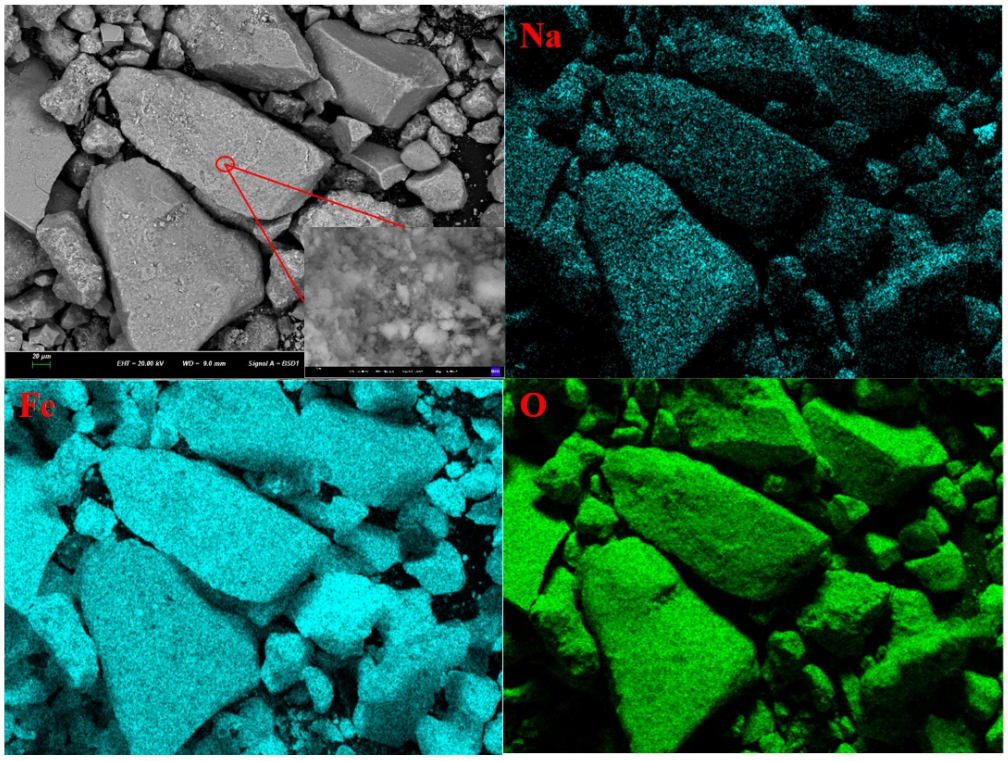

Figure 9. SEM images and EDS element map of the reduction product (2.0% NaOH).

4. Conclusions

In this study, the influence of NaOH content on the reduction kinetics of hematite was investigated systematically through the suspension magnetization roasting technique at the optimum reduction temperature (560 °C). The present research demonstrates that the conversion of hematite to magnetite was strongly inhibited by the addition of NaOH, and the magnetization and specific magnetic susceptibility of the reduction products was significantly decreased with the increase in NaOH content. Even the control step of the reduction of hematite was not affected by the addition of NaOH; its reduction rate was

dramatically decreased by the addition of NaOH. Meanwhile, the apparent activation energy and the pre-exponential factor of the hematite reduction increased significantly from 26.745 kJ/mol to 83.482 kJ/mol and 3.658 min^{-1} to 6987.443 min^{-1}, respectively, after the addition of NaOH from 0% to 2%. Thermodynamic analysis indicated that sodium ferrite could be produced spontaneously under the experimental conditions, and it is hard for it to be further reduced by CO. The SEM-EDS results confirm that the produced sodium ferrite formed a dense film, which covered the surface of hematite particle, and it not only decreased the conversion degree of hematite, but also inhibited the diffusion of CO and thereby hindered the reduction of hematite in the interior.

Author Contributions: Conceptualization, S.Y. and X.W.; methodology, S.Y.; software, X.L.; validation, S.Y., X.W. and Y.L.; formal analysis, H.Z.; investigation, H.Z.; resources, S.Y.; data curation, H.Z.; writing—original draft preparation, X.W.; writing—review and editing, X.W.; visualization, S.Y.; supervision, Y.L.; project administration, X.L.; funding acquisition, S.Y. All authors have read and agreed to the published version of the manuscript.

Funding: This research was funded by [National Natural Science Foundation of China] grant number [52174240; 51904058] and [National Key Research and Development Program of China] grant number [Nos. 2018YFC1901902].

Conflicts of Interest: The authors declare no conflict of interest.

References

1. Lyu, F.; Hu, Y.; Wang, L.; Sun, W. Dealkalization processes of bauxite residue: A comprehensive review. *J. Hazard. Mater.* **2021**, *403*, 123671. [CrossRef] [PubMed]
2. Archambo, M.; Kawatra, S.K. Red mud: Fundamentals and new avenues for utilization. *Miner. Process. Extr. Metall. Rev.* **2020**, *42*, 427–450. [CrossRef]
3. Yang, Y.; Guo, Y.-Q.; Zhu, W.-S.; Huang, J.-B. Environmental impact assessment of China's primary aluminum based on life cycle assessment. *Trans. Nonferrous Met. Soc. China* **2019**, *29*, 1784–1792. [CrossRef]
4. Lu, G.-Z.; Zhang, T.-A.; Ma, L.-N.; Wang, Y.-X.; Zhang, W.-G.; Zhang, Z.-M.; Wang, L. Utilization of Bayer red mud by a calcification–carbonation method using calcium aluminate hydrate as a calcium source. *Hydrometallurgy* **2019**, *188*, 248–255. [CrossRef]
5. Milačič, R.; Zuliani, T.; Ščančar, J. Environmental impact of toxic elements in red mud studied by fractionation and speciation procedures. *Sci. Total Environ.* **2012**, *426*, 359–365. [CrossRef]
6. Alam, S.; Das, S.K.; Rao, B.H. Characterization of coarse fraction of red mud as a civil engineering construction material. *J. Clean. Prod.* **2017**, *168*, 679–691. [CrossRef]
7. Arroyo, F.; Luna-Galiano, Y.; Leiva, C.; Vilches, L.F.; Fernández-Pereira, C. Environmental risks and mechanical evaluation of recycling red mud in bricks. *Environ. Res.* **2020**, *186*, 109537. [CrossRef]
8. Liu, X.; Han, Y.; He, F.; Gao, P.; Yuan, S. Characteristic, hazard and iron recovery technology of red mud—A critical review. *J. Hazard. Mater.* **2021**, *420*, 126542. [CrossRef]
9. Khairul, M.A.; Zanganeh, J.; Moghtaderi, B. The composition, recycling and utilisation of Bayer red mud. *Resour. Conserv. Recycl.* **2019**, *141*, 483–498. [CrossRef]
10. Liu, Y.; Naidu, R. Hidden values in bauxite residue (red mud): Recovery of metals. *Waste Manag.* **2014**, *34*, 2662–2673. [CrossRef]
11. Yuan, S.; Zhou, W.; Han, Y.; Li, Y. Efficient enrichment of low-grade refractory rhodochrosite by preconcentration-neutral suspension roasting-magnetic separation process. *Powder Technol.* **2020**, *361*, 529–539. [CrossRef]
12. Tang, Z.; Zhang, Q.; Sun, Y.; Gao, P.; Han, Y. Pilot-scale extraction of iron from flotation tailings via suspension magnetization roasting in a mixture of CO and H2 followed by magnetic separation. *Resour. Conserv. Recycl.* **2021**, *172*, 105680. [CrossRef]
13. Zhang, Q.; Sun, Y.; Han, Y.; Li, Y. Pyrolysis behavior of a green and clean reductant for suspension magnetization roasting. *J. Clean. Prod.* **2020**, *268*, 122173. [CrossRef]
14. Tang, Z.; Liu, X.; Gao, P.; Han, Y.; Xu, B. Effective induction of magnetite on suspension magnetization roasting of hematite and reaction kinetics verification. *Adv. Powder Technol.* **2022**, *33*, 103593. [CrossRef]
15. Tang, Z.; Xiao, H.; Sun, Y.; Gao, P.; Zhang, Y. Exploration of hydrogen-based suspension magnetization roasting for refractory iron ore towards a carbon-neutral future: A pilot-scale study. *Int. J. Hydrogen Energy* **2022**, *47*, 15074–15083. [CrossRef]
16. Liu, X.; Gao, P.; Yuan, S.; Lv, Y.; Han, Y. Clean utilization of high-iron red mud by suspension magnetization roasting. *Miner. Eng.* **2020**, *157*, 106553. [CrossRef]
17. Yuan, S.; Liu, X.; Gao, P.; Han, Y. A semi-industrial experiment of suspension magnetization roasting technology for separation of iron minerals from red mud. *J. Hazard. Mater.* **2020**, *394*, 122579. [CrossRef]

18. Zinoveev, D.; Grudinsky, P.; Zakunov, A.; Semenov, A.; Panova, M.; Valeev, D.; Kondratiev, A.; Dyubanov, V.; Petelin, A. Influence of Na_2CO_3 and K_2CO_3 Addition on Iron Grain Growth during Carbothermic Reduction of Red Mud. *Metals* **2019**, *9*, 1313. [CrossRef]
19. Xie, R.; Zhu, Y.; Liu, J.; Wang, X.; Li, Y. Differential collecting performance of a new complex of decyloxy-propyl-amine and α-bromododecanoic acid on flotation of spodumene and feldspar. *Miner. Eng.* **2020**, *153*, 106377. [CrossRef]
20. Wang, X.; Gao, P.; Liu, J.; Gu, X.; Han, Y. Adsorption performance and mechanism of eco-friendly and efficient depressant galactomannan in flotation separation of chalcopyrite and molybdenite. *J. Mol. Liq.* **2021**, *326*, 115257. [CrossRef]
21. Liu, J.; Xie, R.; Zhu, Y.; Li, Y.; Liu, C. Flotation behavior and mechanism of styrene phosphonic acid as collector on the flotation separation of fluorite from calcite. *J. Mol. Liq.* **2021**, *326*, 115261. [CrossRef]
22. Yuan, S.; Zhang, Q.; Yin, H.; Li, Y. Efficient iron recovery from iron tailings using advanced suspension reduction technology: A study of reaction kinetics, phase transformation, and structure evolution. *J. Hazard. Mater.* **2021**, *404*, 124067. [CrossRef] [PubMed]
23. Chen, J.; Zhang, R.; Simmonds, T.; Hayes, P.C. Microstructural Changes and Kinetics of Reduction of Hematite to Magnetite in CO/CO_2 Gas Atmospheres. *Metall. Mater. Trans. B* **2019**, *50*, 2612–2622. [CrossRef]
24. Chithiraputhiran, S.; Neithalath, N. Isothermal reaction kinetics and temperature dependence of alkali activation of slag, fly ash and their blends. *Constr. Build. Mater.* **2013**, *45*, 233–242. [CrossRef]
25. Mozammel, M.; Sadrnezhaad, S.K.; Khoshnevisan, A.; Youzbashizadeh, H. Kinetics and reaction mechanism of isothermal oxidation of Iranian ilmenite concentrate powder. *J. Therm. Anal. Calorim.* **2013**, *112*, 781–789. [CrossRef]
26. Gong, D.; Zhou, K.; Li, J.; Peng, C.; Chen, W. Kinetics of Roasting Reaction Between Synthetic Scheelite and Magnesium Chloride. *JOM* **2019**, *71*, 2827–2833. [CrossRef]
27. Fiúza, A.; Silva, A.; Carvalho, G.; de la Fuente, A.V.; Delerue-Matos, C. Heterogeneous kinetics of the reduction of chromium (VI) by elemental iron. *J. Hazard. Mater.* **2010**, *175*, 1042–1047. [CrossRef]
28. Xiang, J.; Huang, Q.; Lv, W.; Lv, X.; Bai, C. Effects of Pre-Oxidation on the Kinetics of Iron Leaching from Ilmenite in Hydro-chloric Acid Solution. In *Rare Metal Technology 2018*; Kim, H., Westrom, B., Alam, S., Ouchi, T., Azimi, G., Neelameggham, N.R., Wang, S., Guan, X., Eds.; Springer International Publishing: Cham, Switzerland, 2018; pp. 301–307.